Dimensional Changes of Cross-laminated Timber Basement Walls Under Ambient Humidity Variation

Fernanda Bezerra Tomaduci Imamura ,* Yuxiang Chen, Lijun Deng, and Ying Hei Chui

Advancements in cross-laminated timber (CLT) applications have introduced the potential to use it as an alternative to reinforced concrete in basement construction. Understanding dimensional stability is crucial to ensure the reliability and safety of CLT in below-grade environments. An experimental CLT basement was constructed in Edmonton, Canada, and monitored over a period of two years. Field measurements were analyzed to estimate the dimensional changes and understand the deformation modes of the CLT panels resulting from changes in boundary conditions. A supporting laboratory experiment with specimens made from single pieces of dimensional lumber was conducted to establish a basis for comparing field-measured dimensional changes in CLT and determining the effects of cross-lamination on swelling and shrinkage coefficients. The average swelling and shrinkage coefficients calculated for CLT were approximately twice as large as the longitudinal and 20 times smaller than the transverse coefficients obtained from the laboratory experiments on solid wood specimens, indicating the influence of cross-lamination on these coefficients. Four deformation modes were identified based on measurements from field-installed strain gauges. The study provides new insights into the impact of water ingress on the swelling coefficient and the effects of different drying conditions on the shrinkage coefficients of CLT.

DOI: 10.15376/biores.20.2.4568-4589

Keywords: Moisture distribution; Dry-out; Moisture safety; Field study; End grain water absorption

Contact information: Department of Civil and Environmental Engineering, University of Alberta, Edmonton, Alberta, Canada, T6G 1H9; *Corresponding author: fimamura@ualberta.ca

INTRODUCTION

Reinforced concrete basements have long been the most common basement construction solution in low-rise residential buildings in North America. However, cement and concrete production account for 5% to 8% of the global CO₂ emissions, corresponding to 3 to 6% of total greenhouse gas emissions. In the future, CO₂ emissions related to this industry can represent 20% of global carbon emissions by 2050 (Van Deventer *et al.* 2020). On top of that, severe heat loss of concrete basements in cold regions further contributes to greenhouse gas emissions. Cross-laminated Timber (CLT) has attracted global interest due to its ability to offer large-sized panels with a high strength-to-weight ratio and excellent structural stability compared to traditional wood products. Compared to traditional concrete components, CLT panels offer better thermal insulation properties, ease of prefabrication, and, more importantly, a lower environmental impact. Using CLT panels could also help overcome the challenges associated with concrete construction in remote locations. A preliminary life cycle assessment conducted on CLT basements revealed that the global warming potential, measured by carbon dioxide emissions, could

be reduced by nearly 80% over a 50-year life span compared to concrete basements (Daneshvar *et al.* 2022). Several key aspects must be considered to verify the suitability of CLT for basement construction, including the durability of panels in below-grade environments, dimensional changes, and deformations caused by cyclic changes in moisture content and thermal conditions.

As a hygroscopic wood-based product, CLT naturally absorbs and stores moisture when interacting with its surrounding environment. The degree of moisture absorption or release is primarily influenced by relative humidity, with temperature and other environmental factors also playing a role (Karacabeyli and Gagnon 2019). Moisture movement in wood occurs through three primary mechanisms: water vapour diffusion, cell wall water diffusion, and capillary transport. Diffusion involves the net mass transfer due to random molecular motion, which can occur in both the vapour phase and within the wood cell wall. Under constant temperature conditions, the overall diffusion of water through the wood in the hygroscopic range can be mathematically modelled using gradients of different assumed potentials, including concentration, moisture content, vapour pressure, and relative humidity. Liquid water transport in wood depends on an interconnected void network, such as the bordered pits found in softwood species. According to Thybring *et al.* (2022), liquid water moves considerably faster along the longitudinal direction than in the radial and tangential directions, due to the orientation and structure of primary wood cells.

Basements are exposed to humid environments due to their contact with soil moisture, which intensifies during rainfall and snow-thawing events. Consequently, any flaws in the protective waterproofing barriers can allow moisture to penetrate the CLT panels. Unlike above-grade CLT structures, the external surface of basement CLT panels is not exposed to outdoor air. It can only dry through exposure to the internally controlled air within the basement.

A primary consideration in the application of wood construction, particularly in basement systems, is the hygric behavior of the material, originating from its inherent susceptibility to moisture-induced degradation (Kukk *et al.* 2022). From a dimensional stability point, wood exhibits anisotropic behaviour, undergoing the most significant shrinkage or swelling in the tangential direction (parallel to the annual growth rings), about half as much in the radial direction (perpendicular to the rings), and minimal changes along the longitudinal direction (parallel to the grain) (Glass and Zelinka 2010).

Indirect damage mechanisms arise from moisture-dependent shrinkage and swelling, as well as the reduction in strength caused by high moisture content. Although these factors may not cause immediate material damage, shrinkage and swelling can lead to cracks along the fibres in the cross-section, potentially compromising the entire component or neighbouring components. Moisture-induced deformations can generate substantial forces within the material (Ott and Aondio 2020). Shirmohammadi *et al.* (2021) further noted that moisture ingress in CLT can compromise structural integrity by causing physical changes that weaken glue bonds and lead to creep and dimensional instability.

Rapid dimensional changes may also result in surface deformations such as splits and checking, thereby compromising the product's functionality and performance. Understanding dimensional stability and the stresses induced by varying environmental conditions throughout the service life of CLT panels is essential to ensuring the long-term reliability, safety, and performance of mass timber structures (Chiniforush *et al.* 2022). Bergman (2010) also mentioned that drying stresses arise from the differential shrinkage

between the outer layer of a board (the shell) and its interior (the core), which can lead to drying defects.

In large CLT panels, the surface layer responds rapidly to changes in moisture content, while the core takes much longer, often weeks or months, to respond to similar environmental changes. Cyclic wetting and drying can cause damage to CLT panels, as repeated swelling and contraction may cause joints and seams to open, allowing water to penetrate beneath the surface and prolonging the drying process (Karacabeyli and Gagnon 2019). Factors such as wood species, grain orientation, and exposure duration significantly affect the rate and extent of water absorption. For example, wood absorbs moisture much faster through its end grain (longitudinal direction) than through transverse directions (Shmulsky and Jones 2019). The end grain joints have been identified as especially vulnerable due to accelerated moisture absorption, as the exposed longitudinal wood fibres readily absorbed bulk water. Kalbe et al. (2022) investigated vertical moisture absorption in CLT structures during construction, revealing that moisture content levels could surpass 25% before commissioning. They also pointed out that most laboratory research involving CLT and bulk water exposure has concentrated on the wetting and drying of panel faces, with limited information available on moisture uptake at the end grain of CLT, moisture intrusion pathways, and methods to prevent end grain wetting. Kalbe et al. (2024) further mentioned that modelling of CLT end grain joints poses challenges because, during liquid water absorption from the bottom end grain surface, there will be layers where the water uptake occurs mainly in the longitudinal direction and layers where it will occur mainly in the transversal direction. At the same time, there will be moisture redistribution within and between the layers. They observed a multi-phase moisture transport: water absorption along the grain in the outer layer while water vapor movement perpendicular to the grain from the surface of the same layer.

Using prefabricated CLT panels as basement walls can reduce construction time and energy consumption over the building's expected lifetime. The main advantages of using CLT in basement construction include the use of renewable materials to make the panels, lower global warming potential, and carbon sequestration. CLT basements can also provide a warmer and more thermally efficient living environment in cold regions.

This paper examines the dimensional changes, swelling coefficients, and shrinkage coefficients in Spruce-Pine-Fir (SPF) CLT panels produced in Western Canada under actual boundary conditions of basements in a cold climate - Edmonton, Alberta. The analysis accounts for moments with different moisture transport and drying conditions. The deformation of the CLT panels due to moisture uptake and dry-out was observed. This paper presents a pioneer study on CLT as a sustainable basement solution. It provides new insights into the effects of moisture-induced strains on the deformation of CLT basement walls. The research program was not intended to study the long-term durability of CLT with respect to biodegradation sources such as termites and decay, nor to develop a new water protection system. Current water protection solutions were used in this experimental basement construction. Other ongoing CLT basement research includes assessing the durability of the CLT panel as basement walls by determining the mould growth risks, as presented by Imamura *et al.* (2024), as well as evaluating the thermal performance of CLT basement walls and estimating essential thermal parameters for energy-saving analyses.

RESEARCH METHODOLOGY

The dimensional changes, swelling and shrinkage coefficients, and deformation modes were estimated using data from a field experimental CLT basement construction, supported by a complimentary laboratory experiment. The CLT basement walls were instrumented and monitored in the field from June 2022 to June 2024. Relative humidity, temperature, and strain data were collected to estimate the swelling and shrinkage coefficients. Deformation data and visual inspections were used to assess the deformation modes and panel dimensional changes. A supporting laboratory experiment was conducted to determine the swelling and shrinkage coefficients using a solid wood specimen made from dimensional lumber of the same species as the CLT panels, Spruce-Pine-Fir.

Field Experiment

Imamura et al. (2024) describe a full-scale CLT basement field experiment measuring 6 m in length (formed by connecting 2 panels measuring 3 m in length), 3 m in width, and 2.4 m in height, with 1.8 m of backfilling built to represent a typical home basement. The basement entrance sits above ground level on the facility's west side, with the door facing west and opening into an elevated entry platform, accessible by a step ladder leading to the basement interior. The CLT panels, 105 mm thick and 3-ply with vertical lumber in both the exterior and interior plies, were selected according to the backfilling height and earth pressure diagram. The structural design calculations were presented in Daneshvar et al. (2022). The panels were connected at the corners with a double row of 220-mm-long self-tapping screws, spaced every 50 mm along the panel height. The joints between panels, forming the longer walls, were connected with 140-mmlong self-tapping screws installed in a staggered pattern at a 45° angle, spaced every 20 mm along the panel height. The connection between the CLT panels and the floor was made with brackets and nails. The basement floor was composed of ½" (1.25 cm) thick plywood boards nailed on top of 2 x 6 (38 x 140 mm) dimensional lumber, spaced every 60 cm, and insulated with a 5 cm thick layer of rigid insulation (EPS). The CLT panels were installed on top of a base plate made of dimensional lumber (2 x 12 nominal) measuring 38 x 292 mm. The base plate was placed directly on the ground.

The exterior surfaces of the basement panels, in contact with the backfilled soil, were covered with a 7.5-cm-thick layer of rigid insulation for thermal protection and a waterproofing membrane for moisture protection. However, the wood end grain was not protected against moisture. A granular layer and a perimeter drain connected to a sump pump were incorporated into the drainage system to ensure proper water management. The two longest walls were selected as the Test Walls. Test Wall 1 was protected with a plastic dimpled waterproofing membrane, while Test Wall 2 was covered with an asphalt-based self-adhesive membrane, and the narrow walls were protected with a fluid-applied membrane that had previously been tested in the laboratory. Figure 1 displays a cross-section including the assembly elements and the basement dimensions.

The CLT experimental basement was constructed at the University of Alberta's south campus farm in Edmonton, Alberta, Canada. The soil at the site represents typical soils found across much of Alberta. Imamura *et al.* (2023) show more details on the site and site investigation.

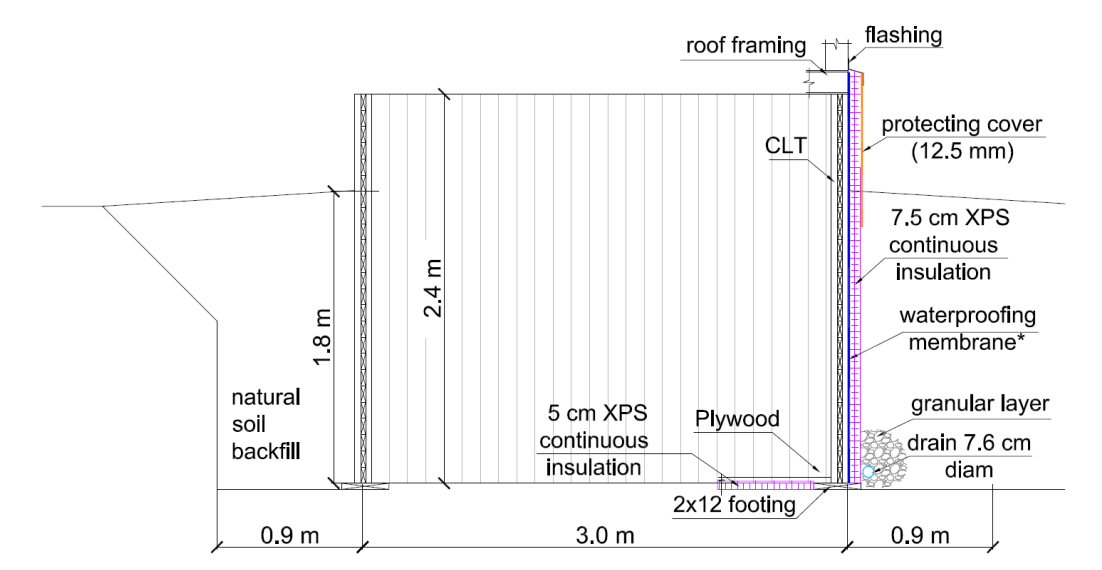


Fig. 1. Experimental CLT basement cross-section

Measurements of relative humidity, temperature, and deformation were obtained from strain gauges and linear variable differential transformers (LVDT) installed at various depths with the Test Walls. Relative humidity and temperature sensors were inserted inside the CLT panel at 2.5 cm and 6.35 cm depth from the internal surface. Figure 2 shows the locations of the sensors in cross-sections. Sixteen strain gauges, type PFLW-30-11-6LJCT-F, 30 mm long from the Tokyo Measuring Instruments Lab, were installed with sixteen 4WFBS120-ohm modules to form a Wheatstone quarter bridge circuit to measure the strain in the CLT panels. Additionally, six LVDTs from Novotechnik, model TEX-0125-421-002-101, 125 mm long, were selected to measure the deflection of the CLT panel. Eighteen relative humidity sensors (relative humidity modules) from TE Connectivity Measurement Specialties, type HM1500LF-ND, were installed inside the CLT panel, with one sensor hung from the ceiling to measure the indoor relative humidity. Additionally, thirty-six type T thermocouples were used to measure the CLT panel temperature.

The strain gauges were aligned with the longitudinal direction of the wood grain (the direction of less deformation) and glued using P-2 adhesive, a general-purpose two-component polyester adhesive. To protect the gauges from the below-grade environment, two layers of protective coatings were applied, as recommended by the manufacturer. The first layer of protection was the SB tape, a white rubber pressure-sensitive butyl membrane. The second was VM tape, a similar material as the SB tape but black in colour with greater width and a polished finish.

A pair of relative humidity sensors and thermocouples were placed inside the CLT wall to collect data for calculating moisture content. The selected relative humidity sensors featured a polymer structure with ±3% accuracy. The RH sensor and thermocouples were inserted into cavities drilled to match their size, minimizing gaps, and the remaining space was sealed with transparent silicone sealant to ensure proper insulation and protection. A data acquisition system was set up, consisting of a CR3000 mini logger, a CR310 datalogger, and AM16/32B multiplexers, to connect and manage the sensors. This system was designed to enable remote data collection through the mobile network (Imamura *et al.* 2024).

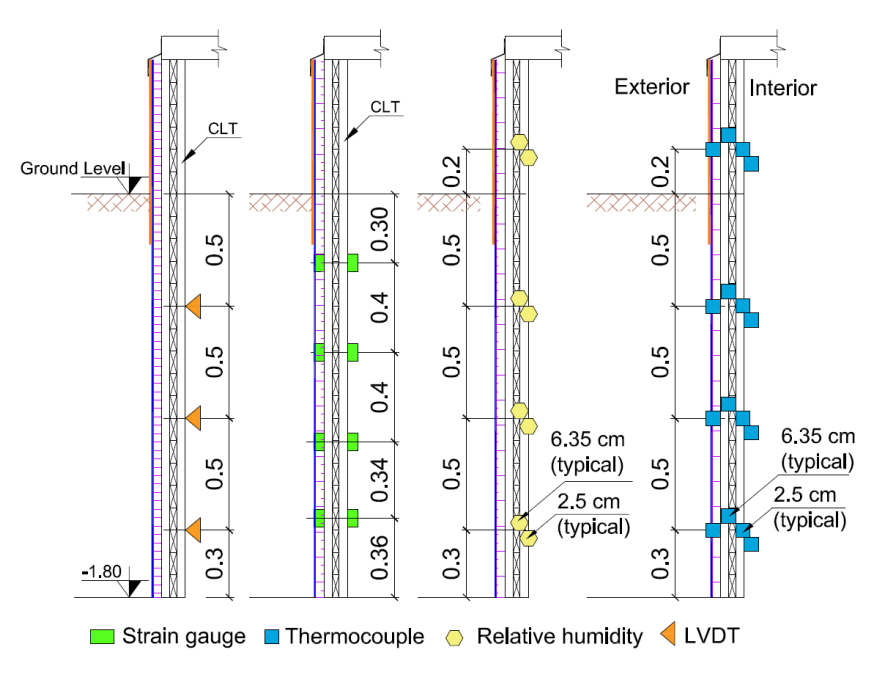


Fig. 2. Instrumentation plan: cross-sections of one Test Wall; Quantities reflect the total number of sensors for both walls

The field construction was finalized in December 2021. The sensor installation was completed in April 2022. However, from April to June, instabilities with the data acquisition system impaired the collection of reliable results. After stabilizing the system, which collects information from 76 instruments every 30 minutes, readings started to be analyzed. The indoor environment of the basement was not climate-controlled. No heating or cooling was regularly provided during the monitoring period. However, during the coldest winter months (January to March), a single small heater without temperature control settings was used to provide heating to the basement. Figure 3 presents photos from the CLT basement construction and depicts the protecting layers applied to the panels. Figure 3a shows the application of the blue seal coat (fluid membrane tested in the laboratory) on a narrow wall. Figure 3b displays the self-adhesive water barrier selected for Test Wall 2.

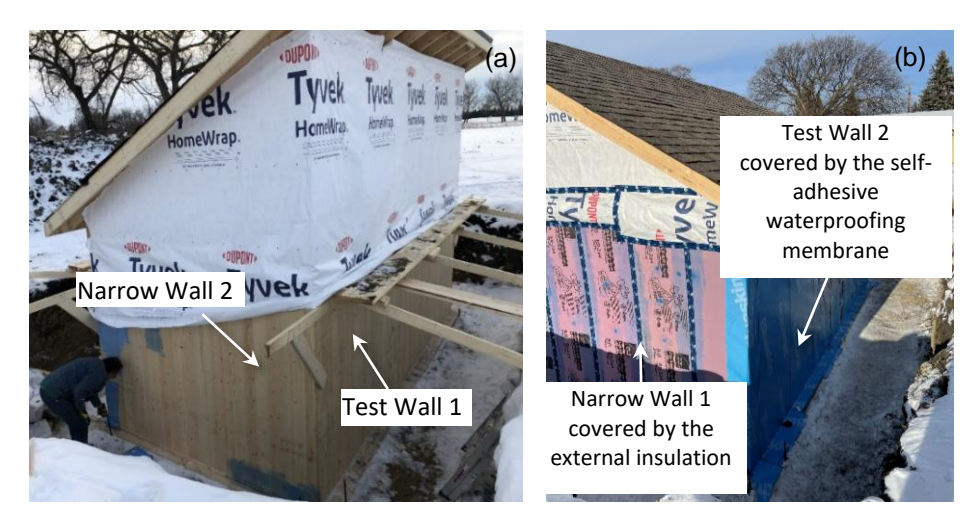


Fig. 3. CLT basement construction: a) applying fluid water protection to the CLT narrow wall 2 in November 2021, b) Test Wall 2 water protection in November 2021

Laboratory Experiment

A laboratory experiment was conducted to determine the shrinkage and swelling coefficients of Spruce-Pine-Fir (SPF) lumber specimens (solid wood) to provide a basis for comparison and to support the evaluation of dimensional changes in the CLT panels based on field experiment data. The idea was to compare the swelling and shrinkage coefficients of the lumber specimen (laboratory) with those of the CLT panels (field) to assess the effects of cross-lamination effects on the swelling and shrinkage of the panels.

The experimental setup involved using small environmental chambers containing saturated salt solutions to create different relative humidity environments, following the ATSM 3069 (2020) standard. A small container was filled with a potassium chloride and water solution to maintain a relative humidity of up to 85%. Another container used magnesium chloride and water solution to achieve 33% relative humidity. In the first set of tests, a temperature and relative humidity logger (onset hobo UX 100-003) was placed inside the chamber to monitor the relative humidity. In the second set of tests, performed six months after the first set of tests, a relative humidity sensor of the same type used in the field experiment, was placed inside the chambers to monitor any changes in humidity during the experiment. The measured air temperature ranged between 21 °C and 22.5 °C, as the laboratory conditions were temperature-controlled. Strain gauges were installed along both the longitudinal and transverse grain directions of two SPF solid wood to measure deformation and determine the swelling and shrinkage coefficients in these directions. The relative humidity sensors and strain gauges used in the laboratory experiment were identical to those used in the field experiment. Figure 4 illustrates the wood grain directions and the location strain gauges on the specimen surface. The SPF lumber produced in western Canada typically consists of Engelmann spruce, white spruce, lodgepole pine, and subalpine fir.

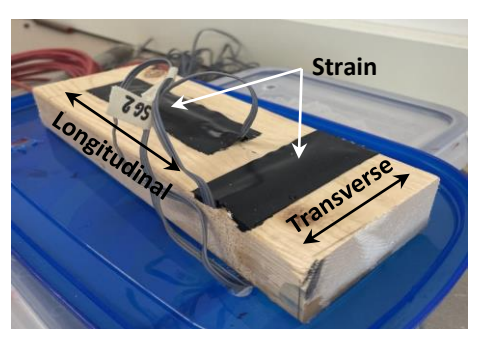


Fig. 4. Measurement of swelling/shrinkage coefficients in two principal directions in lumber specimen.

Five adsorption and five desorption cycles were conducted on the samples, with variations in the initial humidity to which the sample was exposed and the chamber's relative humidity. The initial relative humidity measurements obtained during this experiment represent the chamber's conditions rather than the sample's actual relative humidity at the beginning of each test. When the sample was initially placed in the environmental chamber, its relative humidity was 43%, having equilibrated with the laboratory environment over six months. Tests 5 to 10 (2nd set) were performed six months after Tests 1 to 4 (1st set), allowing the sample's moisture content to re-equilibrate with the laboratory environment before starting the new test cycles. Table 1 shows the laboratory test matrix, highlighting the sample's initial and final relative humidity and the test duration.

Strain, temperature and relative humidity data were measured every 10 min. The equilibrium moisture content (EMC) was calculated using equations based on the relative humidity and temperature measurements, as described by Glass and Zelinka (2010).

Table 1. Laboratory Test Matrix

Test	Specimen	Initial Sample RH (MC) (%)	Final Sample RH (MC) (%)	Duration (h)	Description	
1	1	43 (8.13)	76 (14.81)	340	Adsorption cycle	
2	2	43 (8.13)	81 (16.54)	360	Adsorption cycle	
3	2	81 (16.54)	33 (6.70)	110	Desorption cycle	
4	1	43 (8.13)	30 (6.10)	220	Desorption cycle	
5	1	43 (8.13)	85 (17.88)	350	Adsorption cycle	
6	2	43 (8.13)	35 (6.96)	350	Desorption cycle	
7	1	85 (17.88)	61 (11.15)	220	Desorption cycle	
8	2	35 (6.96)	57 (10.40)	220	Adsorption cycle	
9	1	57 (10.40)	35 (7.01)	840	Desorption cycle	
10	2	59 (10.80)	61 (11.18)	80	Adsorption cycle	

Note: Values in parenthesis represent moisture content (MC)

The samples reached equilibrium moisture content after approximately 300 to 350 hours, depending on the cycle, except for Tests 9 and 10, which took a longer time to reach the equilibrium moisture content. The equilibrium moisture content was not verified using the oven-dry method. Instead, it was estimated by observing the variation in the relative humidity and strain relationship based on the 10-min interval readings. The moisture content during the tests ranged from approximately 7% to 18%. For Tests 9 and 10, a different approach was tried. The plan was to open the chamber lid to allow its relative humidity to equilibrate with the laboratory environment before placing the samples and closing the lid, allowing both the chamber and the samples to gain moisture simultaneously. This approach aimed to increase the sample's moisture content along with the chamber's relative humidity at the same time. However, the chamber conditions were not optimal as interventions to wire the sensors inside disrupted the chamber seal, and the intended outcome was not achieved.

RESULTS

The CLT panels are made by cross-laminating dimension lumber to create strong and stable panels. Moisture movement in CLT presents unique challenges. While the wood still swells and shrinks with changing moisture levels, the glue lines restrict this movement, causing internal stress to develop. This issue is less pronounced during moisture uptake and expansion but becomes more critical during drying. Because cross-lamination influences moisture movement (Shirmohammadi *et al.* 2021), it is essential to understand the dimensional changes of the individual dimension lumber or solid wood of the same species as the CLT panel to compare with field measurements and the swelling and shrinkage coefficients for CLT highlighted in the literature.

Swelling and shrinkage coefficients of solid wood specimens obtained from a laboratory experiment were compared to the swelling and shrinkage coefficients of CLT panels obtained from the field experiment to evaluate the effects of the cross-lamination in constraining dimensional changes.

Due to the anisotropic nature of wood, the shrinkage and swelling coefficients are conventionally expressed in three orthogonal directions, *i.e.*, tangential, radial, and longitudinal (Chiniforush *et al.* 2022). Dimensional changes in wood due to moisture absorption are larger in the tangential direction, approximately twice as much as in the radial direction, depending on the species. However, the highest moisture uptake occurs in the longitudinal direction (Shirmohammadi *et al.* 2021).

Selected dates from the time history series from the field experiment were used to address the deformation modes of the CLT panel. The swelling and shrinkage coefficients were determined from the linear relationship between the measured strain and the change in moisture content from the beginning and end of each laboratory test or cycle once the equilibrium moisture content was achieved. These coefficients were calculated by dividing the change in strain by the corresponding change in moisture content, as shown by Pang and Jeong (2020). The swelling coefficient could be determined by the swelling strain measurement and the adsorption moisture content, as shown in Eq. 1. Similarly, the shrinkage coefficient could be calculated from the measured shrinkage strain and the desorption moisture content, following Eq. 2,

$$S_{w} = \frac{\varepsilon_{SW}}{\Delta MC} \tag{1}$$

$$S_h = \frac{\varepsilon_{sh}}{\Lambda MC} \tag{2}$$

where S_w is the swelling coefficient, S_h is the shrinkage coefficient, ε_{sh} is the shrinkage strain in %, ε_{sw} is the swelling strain in %, and Δ MC in % is the change in moisture content.

Adsorption and Desorption Cycles in Laboratory Experiments

An initial and final strain and the corresponding moisture contents, ranging from approximately 7% to 18%, were recorded from each laboratory test, and the swelling and shrinkage coefficients were determined in two directions relative to the wood grain, the longitudinal and transverse directions, using the linear relationship described by Eqs. 1 and 2. Figure 5a shows the swelling coefficients calculated from the linear relationship for Tests 1, 2, 5, 8, and 10. Figure 5b shows the shrinkage coefficients for Tests 3, 4, 6, 7, and 9 using the same method.

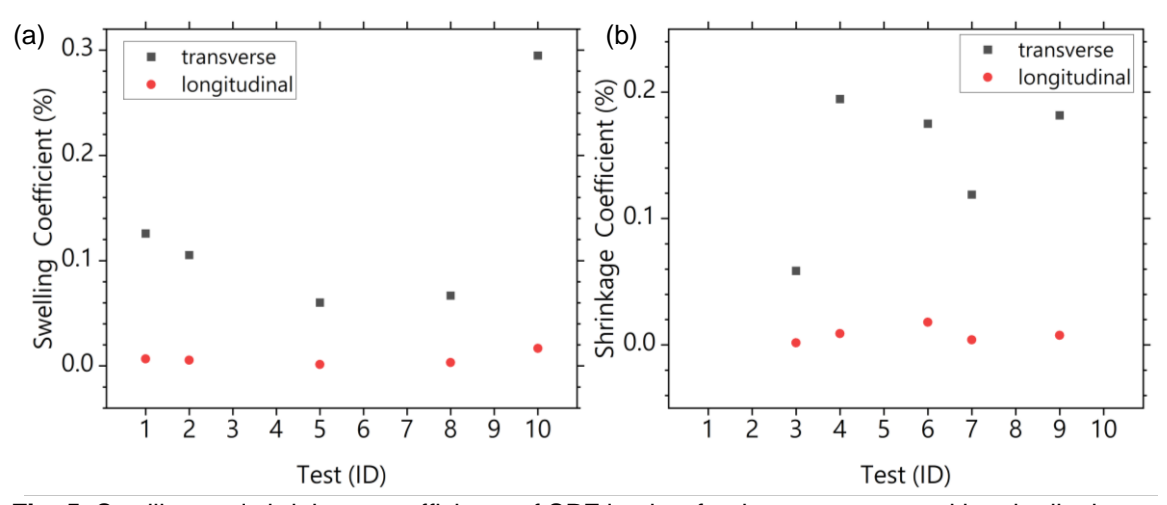


Fig. 5. Swelling and shrinkage coefficients of SPF lumber for the transverse and longitudinal wood directions, using a linear relationship: a) Swelling coefficients, b) Shrinkage coefficients.

The swelling coefficient per 1% moisture content in the transverse directions ranged from 0.060% to 0.295%. However, the results from Test 10 indicate instabilities caused by difficulties in achieving the target relative humidity in the chamber, leading to an unusually high swelling coefficient of 0.295%. Excluding Test 10, the average swelling coefficient was estimated at 0.089%, with a standard deviation of $\pm 0.027\%$. The shrinkage coefficient per 1% moisture content in the same direction ranged from 0.039% to 0.195%, with an average of 0.128% and a standard deviation of ± 0.061 %. In the longitudinal direction, the swelling coefficient ranged from 0.0015% to 0.0067%, not considering the coefficient calculated for test 10, with an average of 0.0042% and a standard deviation of ±0.0020%. In the same direction, the shrinkage coefficient ranged from 0.0008% to 0.018% per 1% moisture content, with an average of 0.0094% and a standard deviation of ±0.006%. According to the literature, the transverse shrinkage coefficient of the SPF species ranges from 6.7% to 7.4%, and the longitudinal coefficient ranges from 0.1% to 0.2% per 1% moisture content, within a moisture content range of 6% to 14% (Glass and Zelinka, 2021). Bengtsson (2001) studied the variation of moisture-induced movements in Norway spruce using 987 specimens made of solid wood and found that the mean swelling coefficient in the longitudinal direction ranged from 0.004% to 0.013%, while in the tangential direction, the coefficient ranged from 0.23% to 0.39%, and in the radial direction, it ranged from 0.10% to 0.22% per % moisture content. The results from the present laboratory experiment align better with the coefficients estimated by Bengtsson (2001) than with those reported by Glass and Zelinka (2021).

Due to methodology differences, the swelling and shrinkage coefficients obtained in the present laboratory experiment may not match the solid SPF wood values reported in the literature. However, because the primary goal of the laboratory experiment was to facilitate a comparison between the solid wood specimens and the CLT panel installed in the field, the coefficients derived served as a valuable reference for the determinations of dimensional changes from the field experiment data. CLT swelling and shrinkage coefficients are affected by cross-lamination and from the field setup, it is not possible to separate the influence of each ply and each wood direction in the measurement of strain. Therefore, the swelling and shrinkage of the CLT panel can be compared to the expected behavior of solid wood made from the same species.

Field Experiment Results

The experimental CLT basement was monitored from June 2022 to June 2024. During this time, significant changes in the moisture content of the CLT panels occurred due to three sump pump failures, which caused moisture uptake through the panel end grain. A heater was used to warm the basement to expedite drying during the winter, causing a significant decrease in relative humidity and moisture content in the panels.

The CLT panel end grain at the bottom was not protected. The panel end rested on a wood footing made of 2×12 lumber (38 mm x 286 mm). After the third sump pump failure, the water level reached around 20 cm above the end grain of the CLT panel and was not removed for around 3 weeks to increase the damage level on the panels for study purposes.

Wetting of CLT end-grain edges is a common issue but has not been well studied. Kalbe *et al.* (2022) reported observations from several buildings experiencing end-grain moisture uptake, where the moisture content often exceeded 25% for several months until targeted heating or drying measures were implemented.

Additionally, vertical plies, forming the internal and external surfaces of the CLT panels (like those used in the present field experiment), exhibited higher moisture contents and slower drying than the horizontal ones, consistent with observations by Kalbe *et al.* (2022).

The wetting and drying process generated significant internal stresses, which could result in internal failures, such as checks or splits running parallel to the grain. Drying stresses, driven by directional differences in shrinkage, can generate internal forces that exceed the wood's material strengths. It is well known that submerged timber absorbs significant amounts of water, leading to swelling and facilitating microbial growth. While such structures can endure rapid drying, presenting warping and checking, the overall structural integrity remains unaffected, provided the wood does not stay wet for extended periods (Shirmohammadi *et al.* 2021).

In March 2024, after 60 days of drying, the CLT panel's internal surface showed some cracks and gaps, as illustrated in Fig. 6. Delamination of parts of the CLT panel was also observed.

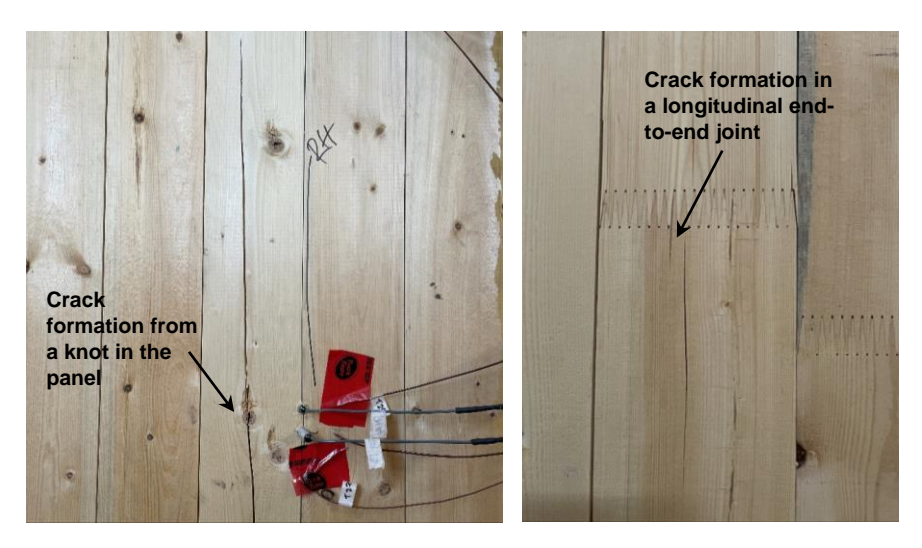


Fig. 6. CLT panel cracks due to low indoor relative humidity

Swelling and Shrinkage Coefficients

The moisture content of CLT panels was calculated using the EMC equation outlined in Glass and Zelinka (2010) based on relative humidity and temperature data collected from both the internal and external surfaces of the CLT panels from sensors installed at 2.5 cm and 6.25 cm inside the panels. Figure 7 presents the moisture content time history for Test Wall 1, representing the collected data and highlighting the dates selected for the dimensional changes and deformation mode analysis. These data points represent the "peaks and valleys" in the relative humidity or moisture content time history for Test Wall 1, corresponding to periods of maximum and minimum relative humidity. These periods also represent moments of different moisture transport within the CLT. When the basement was flooded, liquid water transport was assumed immediately following the sump pump failure, while water vapour diffusion was considered dominant during other moments. For the drying-out periods, a forced dry-out was considered when the basement was heated, and a slow dry-out was considered for the remaining occasions. The sump pump failed thrice, leading to an internal basement flood in July 2022, June

2023, and August 2023. A heater was turned on inside the basement from November 4 to November 13, 2022, and turned off afterward. Another heating cycle started from January 7 until March 16, 2023. From January 5, 2024, to March 15, 2024, the heater was turned on once again. The effects of warming up inside the space are reflected in the decrease in moisture content and a rapid dry-out of the panels.

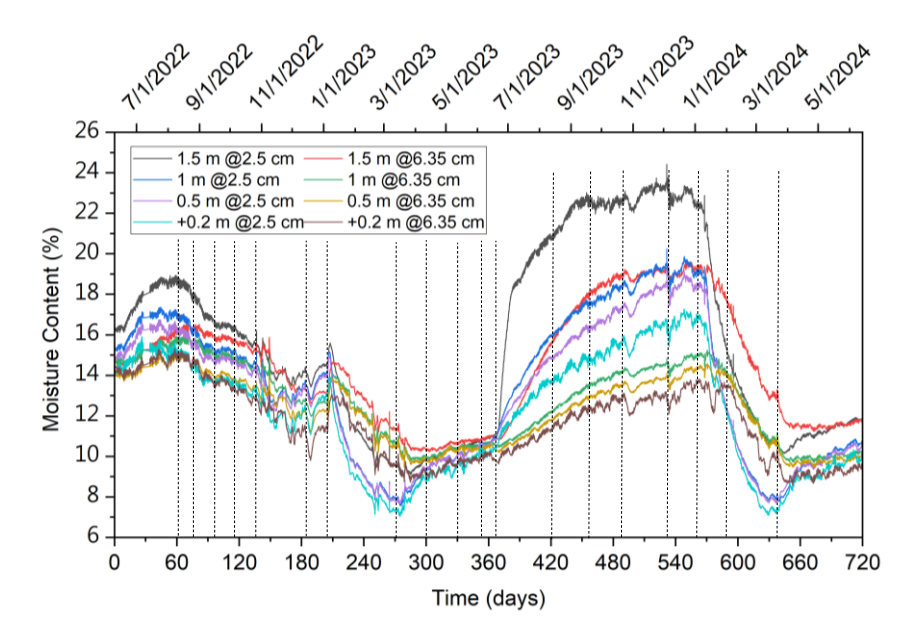


Fig. 7. Moisture content time history for Test Wall 1 indicating the selected dates for a deformation analysis.

Considering both test walls, the moisture content ranged from 7% to 27%. The lowest moisture content corresponded to periods when the basement was heated and the CLT was dried. The highest moisture contents were associated with the sustained high relative humidity after the third sump pump failure in June 2023. The elevated relative humidity levels measured inside the CLT panels indicated abnormal moisture conditions in the basement, reflecting the flooding events.

Strain gauges were installed in the longitudinal direction at four depths at the internal and external surfaces of the CLT panels, as shown in Fig. 2. Figure 8 shows the strain time history for Test Wall 1. The measured strain was corrected for wood thermal expansion, and the remaining strain was assumed to be moisture-induced based on supporting information collected from earth pressure cells installed at the soil-panel interface. Two corrections were necessary: accounting for the wood's thermal expansion and for the strain gauges' thermal compensation. The manufacturer's data sheet provided the thermal compensation indicator for the strain gauges. The wood expansion in the longitudinal direction was estimated as 3.6 microstrains per degree Celsius (°C) for temperatures starting at 0 °C, and this value was subtracted from the strain measurements. For temperatures below 0 °C, wood contraction was assumed to occur at the same rate, although these cases are more complex to evaluate due to potential ice formation. Once the CLT panels were subjected to constant pressure and loads, the panel deformation was mainly due to changes in moisture content. The observed increase and decrease in strain followed a pattern similar to the time history series of relative humidity and moisture content, demonstrating the importance of the moisture changes in the deformation of the panels.

The initial and final strain and corresponding moisture content for each selected time were annotated. The differences between the initial and final values were used to calculate the swelling and shrinkage coefficients using the approach described by Eqs. 1 and 2.

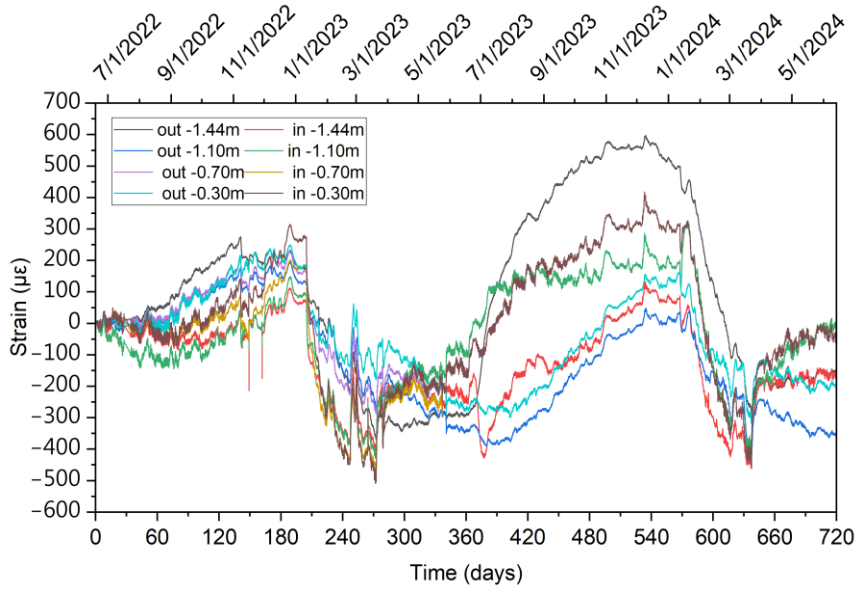


Fig. 8. Strain measurements from Test Wall 1

Although the strain gauges were positioned in the longitudinal direction of the plies, the sensors also captured movement in the transverse direction of the middle layer. The panel was monitored with strain gauges only at the surfaces, and no sensors were installed internally to measure isolated deformations due to moisture uptake. The swelling and shrinkage coefficients derived from these strain measurements accounted for moisture uptake in all directions within the panel, without distinguishing between the uptake in the longitudinal or the transverse direction separately.

The calculation of swelling or shrinkage coefficients assumed equilibrium moisture content conditions and employed a linear relationship between the selected data points to verify deformation due to swelling and shrinkage.

The swelling coefficient was calculated using two conditions: when the panels were exposed to liquid water and when they were exposed to water vapour. Selected data representing these conditions were used to perform the swelling coefficient calculations. The selected dates when the panels were exposed to liquid water were August 16, 2002, June 22, 2023, and August 11, 2023. The dates chosen to illustrate the vapour diffusion moisture transport were April 13, 2023, May 13, 2020, June 2, 2023, September 15, 2023, October 20, 2023, December 4, 2023, and December 29, 2023.

The shrinkage coefficient corresponds to periods during which the moisture content was decreasing. Two data sets were used to estimate this coefficient: periods where the heater was heating the basement and periods without climate control. Data from August 31, 2022, September 20, 2022, October 10, 2022, October 30, 2022, and December 19, 2023, were used to estimate the shrinkage coefficient without climate control. Data from January 3, 2023, March 14, 2023, January 28, 2024, and March 18, 2024, were taken to calculate the shrinkage coefficient for a heated indoor environment. During these periods, the panels achieved very low moisture content and a high strain variation along the panel height, indicating significant shrinkage of the wall during the heat-assisted drying period.

Figure 9 shows the estimated coefficients for Test Wall 1, illustrating the calculated coefficients.

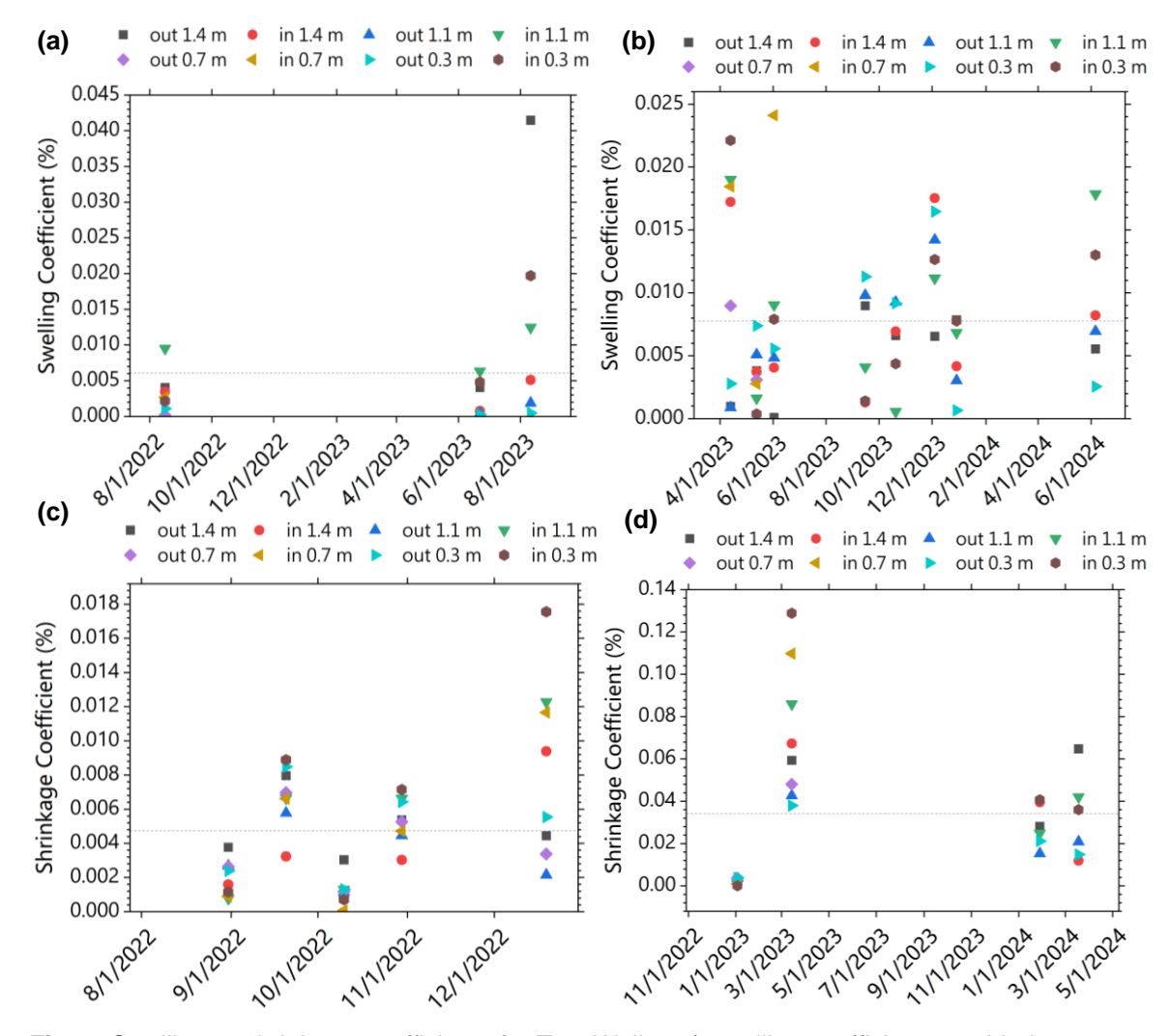


Fig. 9. Swelling or shrinkage coefficients for Test Wall 1: a) swelling coefficient considering a liquid water transport, b) swelling coefficient considering vapour diffusion transport, c) shrinkage coefficient considering slow dry out, d) shrinkage coefficient considering rapid dry out. In the legend, "in" indicates the strain gauge placed at the internal surface of the panel and "out" indicates strain gauges placed at the external surface of the panels.

For Test Wall 1, the minimum swelling coefficient considering liquid water transport in the panels through the CLT end grain was 0.00013%, and the maximum was 0.0415% with an average of 0.0061% per 1% moisture content change. Considering vapour water diffusion, the maximum calculated swelling coefficient was 0.00019%, and the maximum was 0.0178%, with an average of 0.0077%. For Test Wall 2, the minimum swelling coefficient considering liquid water transport was 0.0000606%, and the maximum was 0.0175%, with an average of 0.0.0053% per 1% moisture content change. Considering vapour water diffusion, the maximum calculated swelling coefficient was 0.000187%, and the maximum was 0.0349%, with an average of 0.0078%, the same as the computed coefficient for Test Wall 1 for this type of moisture transport.

For Test Wall 1, the minimum shrinkage coefficient with no climate control in place was 0.0000811%, and the maximum was 0.0175%, with an average of 0.0047%. The shrinkage coefficient calculated for the periods when the basement was heated ranged from 0.00009913% to 0.1288%, a sparse range of values, with an average of 0.034%. For Test Wall 2, the maximum shrinkage coefficient with no climate control was 0.000026%, and the maximum was 0.0166%, similar to Test Wall 1, with an average of 0.00535%. The shrinkage coefficients calculated for the periods where the basement was heated were from 0.000727% to 0.131%, with an average of 0.024%.

Another way to evaluate the swelling and shrinkage coefficients of the CLT panels from the field experiment was to look at the changes with wall depth, as shown in Fig. 10.

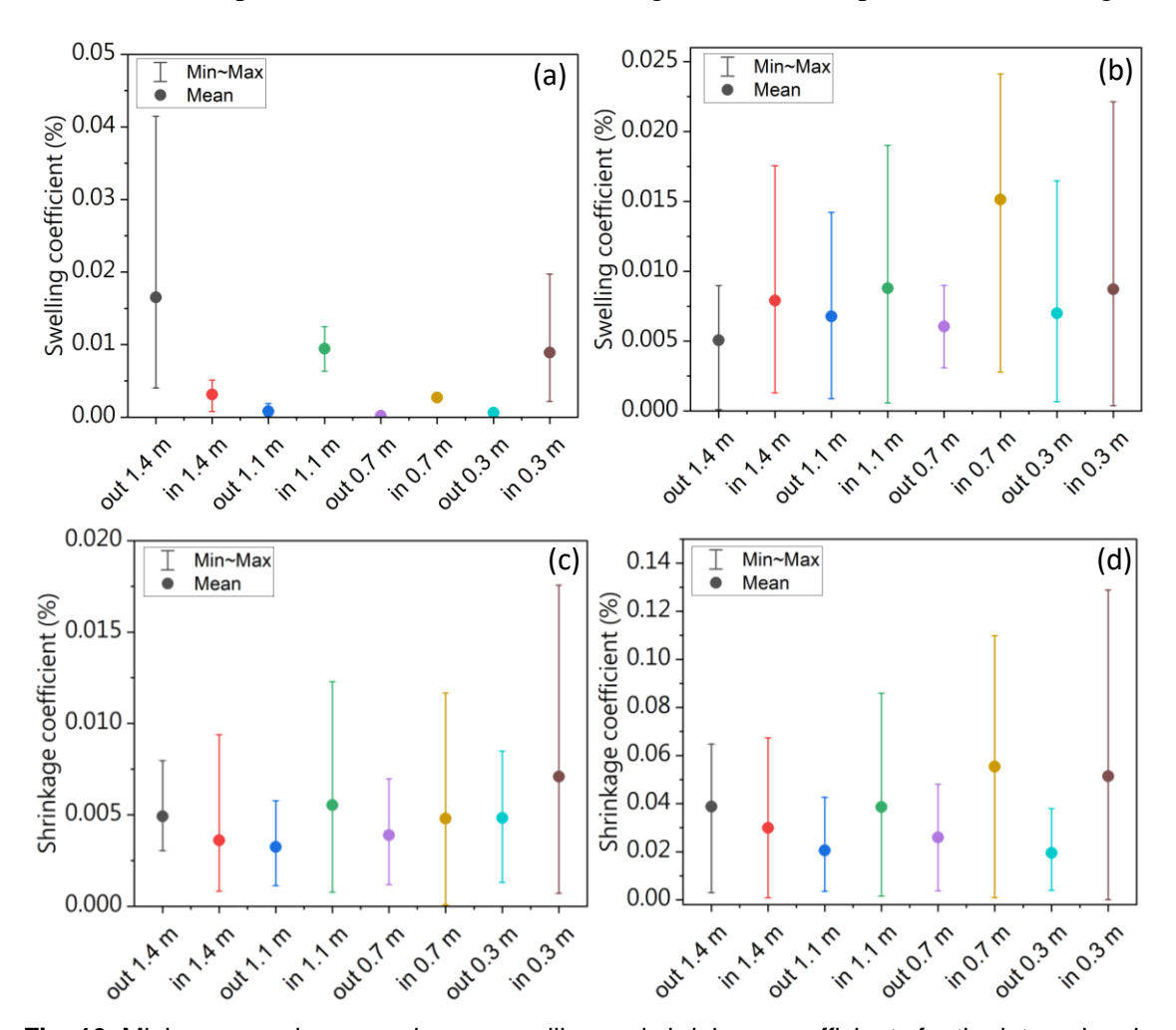


Fig. 10. Minimum, maximum, and mean swelling and shrinkage coefficients for the internal and external surfaces of the CLT panel per depth Test Wall 1: a) swelling coefficient considering a liquid water transport, b) swelling coefficient considering vapour diffusion transport, c) shrinkage coefficient considering slow dry out, d) shrinkage coefficient considering rapid dry out. The error bars display the calculated swelling and shrinkage coefficients' maximum, minimum and mean values.

For swelling coefficients calculated during periods where moisture transport was primarily by water vapour diffusion, 8 values were considered per depth. For swelling coefficients calculated for periods where the moisture transport was mainly due to liquid water, 3 values were considered per depth. For shrinkage coefficients calculated for the

periods with natural dry-out, 5 measurements were taken per depth. For the shrinkage coefficients calculated for the periods where the heater induced the panels to dry out faster, 4 measurements were taken per depth.

The lowest mean swelling coefficients under liquid water transport were found closer to the middle of the panel, while the highest were observed closer to the panel bottom, at 1.5 m below ground level. The moisture content measured at 1.5 m depth was greater than at other depths due to the proximity to the panel end grain, where the moisture uptake was predominantly by liquid water transport. Considering vapour diffusion, the lowest mean swelling coefficient was observed at the bottom of the panel, and the largest was observed at 0.7 m below ground level.

The lowest mean shrinkage coefficient under natural dry-out conditions was observed at 1.10 m below ground level (middle of the panel), and the largest was observed at 0.3 m below ground level (near the top of the panel). Considering the mean shrinkage coefficient observed when the basement was heated, the lowest value was also observed at 1.10 m below ground level and the highest at 0.7 m below ground level.

The wood used in CLT manufacturing typically includes a mix of growth ring orientations, so for cross-sections of most softwood lumber, it is recommended to use an average shrinkage coefficient ranging from 0.2% to 0.25% per 1% change in moisture content (Karacabeyli and Gagnon, 2019). Additionally, the coefficients specified in the European code EN 16351 for CLT are 0.24% in the radial direction (perpendicular to the plane) and 0.02% in the longitudinal direction (in plane) (Pang and Jeong 2020). Table 2 compiles longitudinal and transverse swelling and shrinkage coefficients reported by other authors, tested across different species using different methods.

Table 2. Swelling and Shrinkage Coefficients Estimated from Laboratory Experiments for CLT from Other Authors

Authors	Longitudinal	Transverse	Range of MC	Wood Species	Method
Bengtsson, 2001 in solid wood	0.005% to 0.013%	0.23% to 0.39%	6 to 20%	Norway spruce	RH chamber, caliper
Schwab <i>et</i> al. 1997	0.012% to 0.020%	0.034% to 0.042%	7 to 18%	Norway spruce	-
Gereke et al. 2009	0.009% to 0.022%	0.009% to 0.044%	7 to 24%	European Beech	Digital camera, linear gauge, RH chamber
Brandner 2014	0.02%	0.02%	6 to 22%	Norway spruce	EN 16351
Chiniforush et al. 2022	0.085-0.485/ΔMC (%)	2.30-1.409/ΔMC (%)	7 to 66%	Norway spruce	RH chamber, caliper and moisture meter
Pang and Jeong 2020	0.000095% to 0.00015%	0.000158% to 0.000248%	7 to 30%	Korean Larch	RH chamber, image analysis, and digital image correlation

The maximum shrinkage coefficients calculated from the field experiment during periods when the basement was heated do not agree with previous coefficients estimated by other researchers, being at least ten times larger than the values presented in Table 2. The rapid dry-out of the panels, forced by the heater, may have impacted the methodology, differing from the methods adopted by other authors. The minimum swelling and shrinkage values obtained from the field experiment agree with those reported by Chiniforush *et al.* (2022) and Pang and Jeong (2020). The maximum swelling values from the field experiment align with those of Schwab *et al.* (1997), who measured in the transverse direction, and are consistent with findings from Gereke *et al.* (2009) and Brandner (2014). The average swelling coefficients calculated from the field experiment are lower than most of the values reported in other studies. Discrepancies in the measurements could be attributed to the methodology and boundary control, as it is difficult to control the boundaries in a field experiment.

The CLT panel deformation in the field experiment was measured using strain gauges positioned in the longitudinal wood direction at the internal and external surfaces of the panel. Although the measurements were taken in the longitudinal direction, they may have been affected by the internal transverse moisture uptake and swelling or shrinkage. Therefore, it is not possible to assert that these measurements only reflect the longitudinal swelling and shrinkage. As a result, the field-measured swelling and shrinkage coefficients only represent the overall CLT panel behavior. Comparing the average swelling coefficient calculated from the field experiment for CLT and the average coefficient obtained for the solid wood specimens in the laboratory, the results showed that the field experiment coefficient was 13 times smaller than that obtained from the laboratory experiment, considering the transverse direction of the solid wood specimen.

The average shrinkage coefficient from the field experiment was 25 times smaller than the transverse coefficient from the laboratory experiment. The average shrinkage coefficient from the field experiment for the periods when the basement was heated was 4 times smaller than the transverse coefficient from the laboratory experiment.

The CLT panel swelling and shrinkage coefficients were slightly larger than the longitudinal swelling and shrinkage coefficients for solid wood but significantly smaller than the transverse swelling and shrinkage coefficients. This observation suggests that cross-lamination effectively reduces the swelling and shrinkage of the transverse and radial directions to a reasonable level.

Deformation Modes

The estimated swelling and shrinkage coefficients varied between strain gauges installed at the external and internal surfaces of the CLT panel due to moisture effects. A differential moisture gradient caused deformation differences at these locations due to the panels' moisture uptake and drying. Moisture gradients in wood sections arise when humidity levels vary or deviate from the initial equilibrium. These gradients can be particularly pronounced near the wood's surface, especially during rapid changes in air humidity. They may also be significant within the central regions of the wood sections. Such moisture gradients cause variations in shrinkage and swelling, which, in turn, generate stresses within the wood, known as moisture-induced stresses. The initial moisture content of a timber member is a significant factor. Moisture gradients develop when the air humidity during service deviates substantially from the wood's equilibrium moisture content (Fragiacomo *et al.* 2011).

Four deformation modes for the CLT panel were observed from the strain gauge measurements at the external and internal surfaces for the selected time presented in Fig. 7. Decreasing and increasing strain patterns were used to derive four possible deformations regarding moisture uptake, as illustrated in Fig. 11.

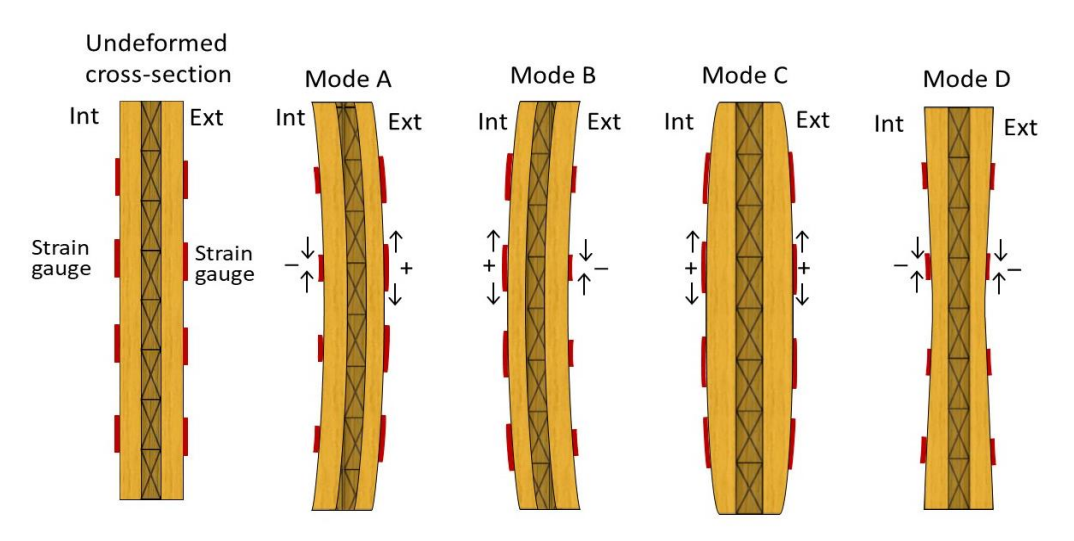


Fig. 11. Deformation modes observed from the strain measurements on the selected dates, previously presented in Fig. 7.

Mode A describes shrinkage and compression of the internal surface of the panel while the external surface swells and is subjected to tension. That could indicate that the moisture distribution across the panel was uneven between the two faces of the panel at the observed times. This deformation mode was observed after 60 days and 720 days of monitoring for Test Wall 1 and after 640 days for Test Wall 2. During this period, the relative humidity and moisture content increased for Test Wall 1 and decreased for Test Wall 2. Mode B describes the opposite behavior: on the internal surface, swelling and tension were observed, while on the external surface, shrinkage and compression were observed. This type of deformation was associated with measurements at 145 days, when the relative humidity and moisture content inside the basement were decreasing for Test Wall 1, and at 60 days, 370 days, and 720 days, when relative humidity and moisture content were increasing for Test Wall 2. Mode C is caused by swelling on both panel surfaces (both sides under tension). This deformation mode was observed during most selected periods for Test Wall 1: at 140 days with decreasing relative humidity, and at 370 days and 535 days with increasing relative humidity. For Test Wall 2, mode C was observed at 140 days and 185 days with decreasing relative humidity and at 535 days with increasing relative humidity. Mode D describes shrinkage and compression on both surfaces of the CLT panel and was observed after 270 days and 640 days when the relative humidity and moisture content decreased considerably for Test Wall 1 and at 270 days with decreasing relative humidity for Test Wall 2.

In May 2023, after 340 days of monitoring, three linear variable differential transformers (LVDT) were installed in each Test Wall after the soil backfilling and compaction to correct for settlement around the basement walls. These sensors were used to estimate the walls' out-of-plane deformation. While strain gauges measured longitudinal strain, LVDTs measured the wall displacement in the out-of-plane direction. Figure 12 shows the deformation time history measured with LVDT for Test Wall 1.

Although the cross-lamination of CLT impacts the deformation analysis because it is difficult to separate the effects of deformation on each ply from the CLT panel, measurements from strain gauges and LVDTs could be analyzed separately to confirm the overall movement of the CLT panel.

The maximum deformation measured by the LVDTs in Test Wall 1 was 3 mm at the center of the wall (1.0 m below ground level), corresponding to a type C deformation mode, which was reached when the basement wall was subjected to a high moisture content resulting from a flood in the basement.

From the deformation measurements, it was possible to capture the wall deformation and movement toward the soil, represented by negative measurements, and toward the basement interior, defined by positive measurements. This could indicate that wall movement was due to shrinkage and swelling, as the deformation trends closely followed the relative humidity and moisture content gain and loss patterns.

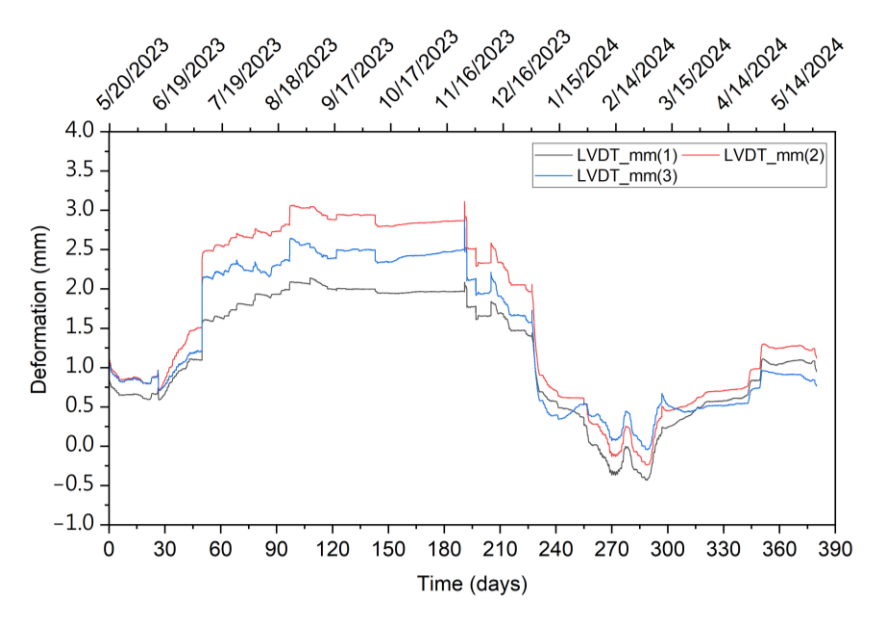


Fig. 12. Deformation time history measured with LVDTs for Test Wall 1. Day 0 in this chart is day 340 of the total monitored data. Positive deflection is towards the interior, and negative deflection is toward the exterior face of the panels.

The deformation was positive when the relative humidity increases, indicating that the panel moves towards the basement interior due to swelling. The deformation decreased, becoming negative when the relative humidity decreased, indicating that the wall shrinks, showing a movement toward the soil. Analyzing the deformation modes over the selected time history, the measurements from LVDTs confirmed the deformation modes derived from the strain gauge measurements.

CONCLUSIONS

Moisture content changes due to humidity and temperature cycles inside basements govern a panel's dimensional changes and deformation. The presented research demonstrated the effects of water transport in wood on the swelling coefficient and the effects of dry-out conditions on the shrinkage coefficients of cross-laminated timber (CLT)

using field measurements. CLT's swelling and shrinkage coefficients, calculated from field measurements under large-scale boundary condition and using strain gauges to measure deformation, were estimated and compared to laboratory measurements from solid wood specimens. Deformation modes were observed from strain measurements, which provided insights into how the external and internal surfaces of the panel were deforming. The main findings are summarized below:

- 1. The CLT swelling and shrinkage coefficients, overall, exhibited values slightly larger than the longitudinal swelling and shrinkage coefficients of solid wood and significantly smaller than the swelling and shrinkage coefficients in the transverse direction of the solid wood, indicating a positive effect of cross-lamination on reducing swelling and shrinkage.
- 2. The most visible dimensional changes observed in the CLT panels through a visual inspection included cracks and delamination. Cracks were most noticeable in areas of the panel surface that contained knots and in the end-to-end joints of the panel lumber.
- 3. Four deformation modes were observed according to the strain measurements and verified with the LVDT measurements. They include swelling in the internal surface with shrinkage of the external face, shrinkage of the internal face with swelling of the external face, swelling on both faces, and shrinkage on both faces. By observing the deformation modes and corresponding moisture content changes in the panels, it was possible to capture the effects of moisture gradients impacting the uneven moisture uptake and drying of the CLT panels.

ACKNOWLEDGEMENTS

The project was funded by Alberta Innovates under the Bio-Opportunities Sub Program (Grant # BFI032). The authors appreciate the guidance and help from Dr. Haitao Yu, the industrial partner at the Landmark Group of Companies, as well as the contributions of Dr. Hossein Daneshvar, Mohammad Fathi, Mohammad Rezvanpour, and Milan Marojevic.

REFERENCES CITED

ASTM E104 (2020). "Standard practice for maintaining constant relative humidity by means of aqueous solutions," ASTM International, West Conshohocken, PA, USA.

Bengtsson, C. (2001). "Variation of moisture-induced movements in Norway spruce (*Picea abies*)," *Annals of Forest Science* 58, 568-581. DOI: 10.1051/forest:2001146

Bergman, R. (2010). "Drying and control of moisture content and dimensional changes," in: *Wood Handbook: Wood as an Engineering Material*, U. S. Department of Agriculture, Forest Products Laboratory, Madison, WI, USA.

Brandner, R. (2014). "Production and technology of cross-laminated timber (CLT): A state-of-the-art report," in: *Proceedings of the Conference: Focus Solid Timber Solutions - European Conference on Cross Laminated Timber (CLT)*, Graz, Austria.

BS EN 16351 (2021). "Timber structures. Cross laminated timber. Requirements," ISBN 9780539002768. BSI.

- Chiniforush, A. A., Ataei, A., Valipour, H. R., Ngo, T. D., and Malek, S. (2022). "Dimensional stability and moisture-induced strains in spruce cross-laminated timber (CLT) under sorption/desorption isotherms," *Construction and Building Materials* 356, Article ID 129252. DOI: 10.1016/j.conbuildmat.2022.129252
- Daneshvar, H., Fakhrzarei, M., Imamura, F., Chen, Y., Deng, L., and Chui, Y. H. (2022). "Structural analysis and design of sustainable cross-laminated timber foundation walls," *Buildings* 12(7), article 979. DOI: 2075-5309/12/7/979#
- Fragiacomo, M., Fortino, S., Tononi, D, Usardi, I., and Toratti, T. (2011). "Moisture-induced stresses perpendicular to grain in cross-sections of timber members exposed to different climates," *Engineering Structures* 33, 3071-3078. DOI: 10.1016/j.engstruct.2011.06.018
- Gereke, T., Schnider, T., Hurst, A, and Niemz, P. (2009). "Identification of moisture-induced stresses in cross-laminated wood panels from beech wood (*Fagus sylvatica L.*)," *Wood Science and Technology* 43, 301-315. DOI: 10.1007/s00226-008-0218-1
- Glass, S. V., and Zelinka, S. L. (2010). "Moisture relations and physical properties of wood," in: *Wood Handbook: Wood as an Engineering Material*, U. S. Department of Agriculture, Forest Products Laboratory, Madison, WI, USA.
- Imamura, F. B. T., Chen, Y., Deng, L. and Chui, Y. H. (2023). "Field research on soil-structure interaction of sustainable basement using mass timber panels," GeoSaskatoon, Saskatoon, Canada.
- Imamura, F. B. T., Chen, Y., Deng, L. and Chui, Y. H. (2024). "Moisture and mould growth risk of cross-laminated timber basement walls: laboratory and field investigation," *Construction and Building Materials* 428, article ID 136150. DOI: 10.1016/j.conbuildmat.2024.136150
- Kalbe, K., Kalamees, T., Kukk, V., Ruus, A., and Annuk, A. (2022). "Wetting circumstances, expected moisture content, and drying performance of CLT end-grain edges based on field measurements and laboratory analysis," *Building and Environment* 221, article ID 10924. DOI: 10.1016/j.buildenv.2022.109245
- Kalbe, K., Parn, R., Ruus, A., and Kalmees, T. (2024). "Enhancing CLT construction Hygrothermal modelling, novel performance criterion, and strategies for end-grain moisture safety," *Journal of Building Engineering* 98, article 111411. DOI: 10.1016/j.jobe.2024.111411
- Karacabeyli, E., and Gagnon, S. (2019). *CLT Handbook* (Special publication SP-532E), FPInnovations, Pointe-Claire, QC, Canada.
- Kukk, V., Kers, J., Kalamees, T., Wang, L., and Ge, H. (2022). "Impact of built-in moisture on the design of hygrothermally safe cross-laminated timber external walls: A stochastic approach," *Building and Environment* 226, article ID 109736. DOI: 10.1016/j.buildenv.2022.109736
- Ott, S., and Aondio, P. (2020). "Observations of moisture damages in historic and modern wooden constructions," in: XV International Conference on Durability of Building Materials and Components, Barcelona, Spain.
- Pang, S. J., and Jeong, G. Y. (2020). "Swelling and shrinkage behaviors of cross-laminated timber made of different species with various lamina thickness and combinations," *Construction and Building Materials* 240, article ID 117924. DOI: 10.1016/j.conbuildmat.2019.117924
- Schwab, E. Steffen, A., and Korte, C. (1997). "In-plane swelling and shrinkage of woodbased panels," *Holz als Roh-und Werkst*. 55(4), 227-233.

- Shirmohammadi, M., Leggate, W., and Redman, A. (2021). "Effects of moisture ingress and egress on the performance and service life of mass timber products in buildings: A review," *Construction and Building Materials* 290, article ID 123176. DOI: 10.1016/j.conbuildmat.2021.123176
- Shmulsky, R., and Jones, P. D. (2019). Forest Products and Wood Science: An Introduction, John Wiley and Sons Ltd., Hoboken, NJ, USA. DOI: 10.1002/9781119426400
- Thybring, E. E., Fredriksson, M., Zelinka, S. L., and Glass, S. V. (2022). "Water in wood: A review of current understanding and knowledge gaps," *Forests* 13, article 2051. DOI: 10.3390/f13122051
- Van Deventer, J. S. J., White, C. E., and Myers, R. J. (2020). "A roadmap for production of cement and concrete with low-CO₂ emissions," *Waste and Biomass Valorization* (12):4745–4775. DOI: 10.1007/s12649-020-01180-5

Article submitted: February 7, 2025; Peer review completed: February 26, 2026; Revised version received and accepted: April 14, 2025; Published: April 29, 2025. DOI: 10.15376/biores.20.2.4568-4589